Fully analytical design of electromagnetic transmissive metagratings for highly efficient extreme-angle beam refraction and reflection

Zhen Tan,[1,2,*] Jianjia Yi,[1,†] Badreddine Ratni,[2] and Shah Nawaz Burokur[2,‡]

[1] *School of Information and Communications Engineering, Xi'an Jiaotong University, Xi'an, 710049, China*
[2] *LEME, UPL, Univ Paris Nanterre, Ville d'Avray, 92410, France*

(Received 4 November 2023; revised 15 December 2023; accepted 16 January 2024; published 5 February 2024)

Metagratings are promising candidates for extreme-angle beam manipulation, due to two main features, namely, the ability to maintain very high efficiency in beam manipulation at extreme angles and the simplicity of the sparsely arranged structure for an easy physical implementation. Here, we propose to design transmissive metagratings, which can achieve highly efficient extreme-angle beam manipulation under normal incidence using a fully analytical design methodology, where information about the positions and impedance density values of the meta-atoms are derived from closed-form expressions. The design methodology is verified by full-wave simulations for extreme-angle anomalous refraction and reflection, where the simulations results are found to be consistent with the theoretical predictions. Proof-of-concept prototypes are fabricated and experimental demonstrations performed around 10 GHz are found to be in good agreement with the simulation results. The proposed metagratings open the door to high-efficiency functionalities in far-field beam manipulations and wireless power transfer.

DOI: 10.1103/PhysRevApplied.21.024009

I. INTRODUCTION

Beam manipulation has always been a key topic in modern wireless communications. Particularly, with the development of fifth-generation (5G) wireless systems, high data throughput of millimeter-wave communications, and the fact that millimeter waves do not propagate well through obstacles, such as walls, efficient beam-manipulation schemes are highly demanded [1]. In the past, phased antenna arrays were commonly used to achieve beam manipulation [2]. With the emergence of artificially engineered structures, the ability to achieve low-cost beam manipulation has become possible [3] and the subsequent development of metasurfaces has enabled beam manipulation with significantly reduced profile structures [4]. While phase gradient metasurfaces based on generalized Snell's law have provided an alternative means of beam manipulation [5], a significant decline in efficiency is observed for large deflection angles due to the mismatch between the wave impedance of incident and outgoing waves [6]. To improve large-angle beam-manipulation efficiency, the concept of Huygens' metasurfaces has been proposed [7]. Based on the equivalence principle, Huygens' metasurfaces enable independent control of electric and magnetic fields of the incident wave through equivalent electric surface admittance and magnetic surface impedance [8–11]. As a result, beam manipulation with perfect beam deflection can be achieved with a passive and lossless Huygens' metasurface [12]. However, the need to tailor two resonances presents a design challenge for the use of such metasurfaces in practical applications due to their complex structure and fabrication processing.

Recently, metagratings have been proposed to achieve beam manipulation with near-unity efficiency [13]. The period of the structure, also known as the supercell, can be designed as a complete scatterer, allowing independent control of multiple diffraction modes and maintaining a high level of efficiency for any diffraction angle. The sparse arrangement of the meta-atoms further allows simple and easy fabrication process [14]. So far, there have been several developments in beam manipulation with metagratings. In Ref. [15], a rigorous analytical methodology for electromagnetic metagratings using microstrip capacitor structure as meta-atoms was proposed. Subsequently, anomalous reflection based on a reflective metagrating was designed using a single meta-atom per supercell with printed-circuit-board (PCB) technology [16,17]. Then, more meta-atoms were introduced into the metagratings supercell to control a large number of diffraction orders, to enable more functionality-rich beam manipulation [18–24]. Later, a semianalytical methodology and an equivalent circuit model were proposed to design arbitrary multilayered metagratings with multiple meta-atoms

*zhzhtan@hotmail.com
†jianjia.yi@xjtu.edu.cn
‡sburokur@parisnanterre.fr

per period to achieve versatile beam manipulation [25, 26]. While for a metagrating containing a large number of meta-atoms per period, numerical optimization is a good means to finalize the design due to the complex field coupling, for basic beam-manipulation functionality, which usually require only a few number of meta-atoms per period, a fully analytical design can circumvent numerical optimization to facilitate the design procedure [27–29].

In this work, we propose a fully analytical methodology to design transmissive metagratings, which can efficiently achieve beam manipulations at arbitrary extreme angles under normal incident wave illumination. Compared to previous analytical or numerical techniques for realizing similar beam manipulations [25,30], the proposed fully analytical procedure presents the advantage to be a more straightforward and intuitive theoretical tool to accomplish the design. In particular, the locations of the meta-atoms as well as the purely imaginary load impedance for realizing desired beam manipulation can be directly calculated by the closed-form load-impedance relations, and the choice of the substrate thickness, which plays a role in Ohmic losses, can be directly avoided. Compared to designs previously accomplished with genetic algorithms [30], the metagratings designed in this study have fewer meta-atoms, making the structure of the metagratings simpler and sparser. Interestingly, anomalous beam reflection is tailored from a metagrating topology without ground plane and is experimentally verified from a transmissive metagrating in this study. Finally, the analytical formulas presented in the paper can be expected to facilitate the application of metagratings in future antennas as well as wireless communication systems [31,32].

II. THEORY

The schematic of extreme-angle beam manipulation based on electromagnetic metagratings is shown in Fig. 1(a). Highly efficient beam manipulation at any extreme angle can be achieved when the metagrating is illuminated by a TE-polarized ($E_y = E_z = H_x = 0$) electromagnetic wave. The considered metagrating is a two-dimensional structure, which is invariant along the x direction and exhibits a periodic alignment in the y direction. The distance between the upper and lower surfaces along the z direction is h. The side view of the supercell (period with length Λ_y) composing the metagrating with the established coordinate system is shown in Fig. 1(b). The supercell contains five wires, three of which are located on the upper layer of the dielectric substrate and two on the lower layer, and their constellations are $(y_1, z_1) = (-d_1, h)$, $(y_2, z_2) = (0, h)$, $(y_3, z_3) = (d_2, h)$, $(y_4, z_4) = (-d_3, 0)$, and $(y_5, z_5) = (d_4, 0)$. Here, (y_i, z_i) $(i = 1, 2, 3, 4, 5)$ denote the coordinates of each wire in Fig. 1(b), respectively. We consider the groundless metagrating with air above ($z < -h$) as well as below ($z > 0$), and the permittivity of air and dielectric substrate are ε_0 (ε_0 is the permittivity of vacuum) and $\varepsilon_s = \varepsilon_r \varepsilon_0$ (ε_r is the relative permittivity of the substrate), respectively. Since both air and dielectric substrate are nonmagnetic media, the wave number and wave impedance in the air and substrate are $k_0 = \omega\sqrt{\mu_0\varepsilon_0}$, $\eta_0 = \sqrt{\mu_0/\varepsilon_0}$, $k_s = \omega\sqrt{\mu_0\varepsilon_s}$, and $\eta_s = \sqrt{\mu_0/\varepsilon_s}$, respectively.

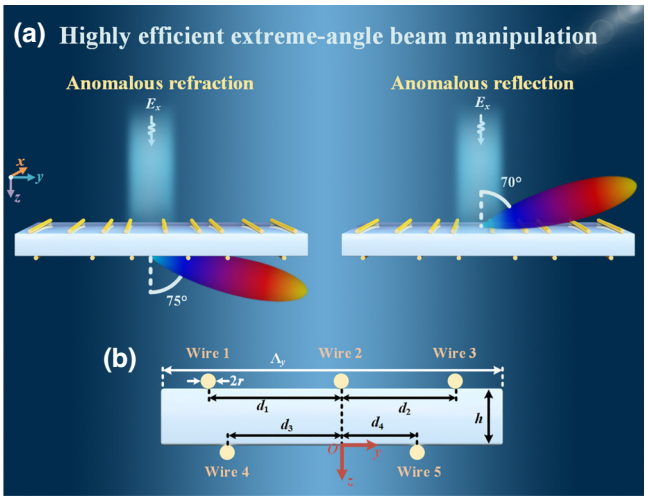

FIG. 1. (a) Schematic of extreme-angle beam manipulation based on electromagnetic metagratings. (b) Side view of the supercell composing the metagratings.

When considering a TE-polarized electromagnetic wave of amplitude E_{in} the transmissive metagrating illuminating at an incident angle θ_{in} and ignoring the time factor $e^{j\omega t}$, a number of diffraction modes is generated. The external field (incident field plus reflected field) in the upper half-space ($z \le -h$) can be written as

$$E_x^{\text{ext}}(y,z) = E_{\text{in}}[e^{-j\beta_0(z+h)} + R_0 e^{j\beta_0(z+h)}]e^{-j\xi_0 y}, \quad (1)$$

where $\xi_0 = k_0 \sin\theta_{\text{in}}$ and $\beta_0 = k_0 \cos\theta_{\text{in}}$ are the transverse and longitudinal wave numbers of the incident wave in air and k_0 is given as $k_0 = 2\pi/\lambda_0$ (λ_0 is the wavelength corresponding to the operating frequency in vacuum). The external field (transmitted field) in the lower half-space ($z \ge 0$) is written as

$$E_x^{\text{ext}}(y,z) = E_{\text{in}} T_0 e^{-j\xi_0 y} e^{-j\beta_0 z}, \quad (2)$$

where R_0 and T_0 in Eqs. (1) and (2) are the Fresnel reflection and transmission coefficient of the incident wave, respectively, and given as

$$R_0 = \frac{j(1-\rho_0^2)\sin(\beta_s h)}{2\rho_0\cos(\beta_s h) + j(1+\rho_0^2)\sin(\beta_s h)}, \quad (3)$$

$$T_0 = \frac{2\rho_0}{2\rho_0 \cos(\beta_s h) + j\,(1+\rho_0^2)\sin(\beta_s h)}, \tag{4}$$

where $\beta_s = \sqrt{k_s^2 - (k_0 \sin\theta_{\text{in}})^2}$ is the longitudinal wave number of the incident wave in the dielectric substrate, k_s is written as $k_s = \sqrt{\varepsilon_r} k_0$, and ρ_0 is defined as $\rho_0 = \beta_s/\beta_0$. Equations (3) and (4) can be derived by the tangential continuity of the electromagnetic field at the upper and lower interfaces of the metagrating.

Next, we analyze the radiation fields of the metagrating located in the upper and lower layers of the dielectric substrate. We use I_1^u, I_2^u, and I_3^u to denote the line currents on the upper wires and I_1^l and I_2^l denote wires in the lower layer of the supercell. The radiation field of the metagrating in the upper half-space ($z \le -h$) is [33]

$$E_x^u(y,z) = -\frac{\eta_0 k_0}{4} \sum_{n=-\infty}^{\infty} e^{-j\xi_0 n\Lambda_y} [I_1^u H_0^{(2)}(k_0 l_1^u) + I_2^u H_0^{(2)}(k_0 l_2^u) + I_3^u H_0^{(2)}(k_0 l_3^u)] \tag{5}$$

with

$$l_1^u = \sqrt{(z+h)^2 + (n\Lambda_y - d_1 - y)^2}, \tag{6a}$$

$$l_2^u = \sqrt{(z+h)^2 + (n\Lambda_y - y)^2}, \tag{6b}$$

$$l_3^u = \sqrt{(z+h)^2 + (n\Lambda_y + d_2 - y)^2}, \tag{6c}$$

where $H_0^2(\cdot)$ is the second kind Hankel function. Similarly, the radiation field of the metagrating in the lower half-space ($z \ge 0$) is

$$E_x^l(y,z) = -\frac{\eta_0 k_0}{4} \sum_{n=-\infty}^{\infty} e^{-j\xi_0 n\Lambda_y} [I_1^l H_0^{(2)}(k_0 l_1^l) + I_2^l H_0^{(2)}(k_0 l_2^l)] \tag{7}$$

with

$$l_1^l = \sqrt{z^2 + (n\Lambda_y - d_3 - y)^2}, \tag{8a}$$

$$l_3^l = \sqrt{z^2 + (n\Lambda_y + d_4 - y)^2}. \tag{8b}$$

For a clearer analysis of the radiation field of the currents array, Poisson's summation formula with the Fourier variation of the Hankel function is used to rewrite the above Eqs. (5) and (7) in the form of a superposition of Floquet-Bloch modes [33]

$$E_x^u(y,z) = -\sum_{m=-\infty}^{\infty} \frac{k_0 \varsigma_m^u}{\beta_m} e^{-j\xi_m y} e^{-j\beta_m |z+h|}, \tag{9}$$

$$E_x^l(y,z) = -\sum_{m=-\infty}^{\infty} \frac{k_0 \varsigma_m^l}{\beta_m} e^{-j\xi_m y} e^{-j\beta_m |z|} \tag{10}$$

with

$$\varsigma_m^u = \frac{\eta_0}{2\Lambda_y}(I_1^u e^{-j\xi_m d_1} + I_2^u + I_3^u e^{j\xi_m d_2}), \tag{11}$$

$$\varsigma_m^l = \frac{\eta_0}{2\Lambda_y}(I_1^l e^{-j\xi_m d_3} + I_2^l e^{j\xi_m d_4}), \tag{12}$$

where $\xi_m = k_0 \sin\theta_{\text{in}} + (2\pi m/\Lambda_y)$ and $\beta_m = \sqrt{k_0^2 - \xi_m^2}$ are the transverse and longitudinal wave numbers of the mth-order Floquet mode in air, respectively.

When considering the reflection as well as transmission of the line currents' radiation field in the substrate, the superposed radiation field of the line currents array (incident field is not included here) in the upper half-space of the substrate ($z \le -h$) is

$$E_x^{\text{rad}}(y,z) = -k_0 \sum_{m=-\infty}^{\infty} \left(\frac{1+R_m}{\beta_m}\varsigma_m^u + \frac{T_m}{\beta_m}\varsigma_m^l\right) \times e^{-j\xi_m y} e^{-j\beta_m |z+h|} \tag{13}$$

and the superposed radiation field in the lower half-space ($z \ge 0$) of the substrate is

$$E_x^{\text{rad}}(y,z) = -k_0 \sum_{m=-\infty}^{\infty} \left(\frac{1+R_m}{\beta_m}\varsigma_m^l + \frac{T_m}{\beta_m}\varsigma_m^u\right) \times e^{-j\xi_m y} e^{-j\beta_m z}, \tag{14}$$

where R_m and T_m are the Fresnel reflection and transmission coefficients of the mth diffraction mode, respectively, which can be obtained through the tangential continuity of the electromagnetic field at the upper ($z = -h$) and lower ($z = 0$) interfaces of the metagrating, written as

$$R_m = \frac{j\,(1-\rho_m^2)\sin(\beta_{ms} h)}{2\rho_m \cos(\beta_{ms} h) + j\,(1+\rho_m^2)\sin(\beta_{ms} h)}, \tag{15}$$

$$T_m = \frac{2\rho_m}{2\rho_m \cos(\beta_{ms} h) + j\,(1+\rho_m^2)\sin(\beta_{ms} h)} \tag{16}$$

with $\beta_{ms} = \sqrt{k_s^2 - \xi_m^2}$, and $\rho_m = \beta_{ms}/\beta_m$. Here, Eqs. (15) and (16) are the generalized forms of Eqs. (3) and (4).

Combining Eqs. (1) and (13), the total field in the upper half-space ($z \le -h$) of the metagrating can be expressed as

$E_x^{\text{tot}} = E_x^{\text{ext}} + E_x^{\text{rad}}$, which is written as

$$E_x^{\text{tot}}(y,z) = E_{\text{in}} e^{-j\beta_0(z+h)} e^{-j\xi_0 y} + \sum_{m=-\infty}^{\infty} E_m^u e^{-j\xi_m y} e^{j\beta_m(z+h)}. \tag{17}$$

Similarly, combining Eqs. (2) and (14), the total field in the lower space ($z \geq 0$) of the metagrating can be written as

$$E_x^{\text{tot}}(y,z) = \sum_{m=-\infty}^{\infty} E_m^l e^{-j\xi_m y} e^{-j\beta_m z}, \tag{18}$$

where E_m^u and E_m^l are the amplitudes of the mth-order diffraction mode of the reflection and transmission, respectively, which can be denoted as

$$E_m^u = -k_0 \left(\frac{1+R_m}{\beta_m} \varsigma_m^u + \frac{T_m}{\beta_m} \varsigma_m^l \right) + \delta_{m0} E_{\text{in}} R_0, \tag{19}$$

$$E_m^l = -k_0 \left(\frac{1+R_m}{\beta_m} \varsigma_m^l + \frac{T_m}{\beta_m} \varsigma_m^u \right) + \delta_{m0} E_{\text{in}} T_0, \tag{20}$$

where δ_{m0} is the Kronecker function.

Under normal incidence, for $\lambda_0 < \Lambda_y < 2\lambda_0$, the transmissive metagratings have six diffraction modes (three reflection modes and three transmission modes), which is sufficient to meet the requirement for extreme-angle beam manipulation (see Appendix A for details). First, for these propagating diffraction modes, we have [28]

$$P_m^u = \frac{|E_m^u|^2 \beta_m}{|E_{in}|^2 \beta_0}, \quad P_m^l = \frac{|E_m^l|^2 \beta_m}{|E_{in}|^2 \beta_0}, \tag{21}$$

$$\sum_{m=-1}^{1} P_m^u + \sum_{m=-1}^{1} P_m^l = 1, \tag{22}$$

where P_m^u and P_m^l denote the power ratio accounted for by the mth reflection diffraction order and the mth transmission diffraction order, respectively.

According to the above Eq. (21), the amplitude of the mth-order propagating diffraction modes can also be written as

$$E_m^u = e^{j\varphi_m^u} E_{\text{in}} \sqrt{P_m^u \beta_0 / \beta_m}, \tag{23}$$

$$E_m^l = e^{j\varphi_m^l} E_{\text{in}} \sqrt{P_m^l \beta_0 / \beta_m}. \tag{24}$$

Thus, combining Eqs. (19), (20), (23), and (24), we can get

$$-\frac{\eta_0}{2\Lambda_y} \left[(1+R_m) \left(I_1^u e^{-j\xi_m d_1} + I_2^u + I_3^u e^{j\xi_m d_2} \right) + T_m \left(I_1^l e^{-j\xi_m d_3} + I_2^l e^{j\xi_m d_4} \right) \right] + \delta_{m0} E_{\text{in}} R_0 = E_{\text{in}} e^{j\varphi_m^u} \sqrt{P_m^u \beta_{\text{m}} / \beta_0}, \tag{25}$$

$$-\frac{\eta_0}{2\Lambda_y} \left[(1+R_m)(I_1^l e^{-j\xi_m d_3} + I_2^l e^{j\xi_m d_4}) + T_m (I_1^u e^{-j\xi_m d_1} + I_2^u + I_3^u e^{j\xi_m d_2}) \right] + \delta_{m0} E_{\text{in}} T_0 = E_{\text{in}} e^{j\varphi_m^l} \sqrt{P_m^l \beta_{\text{m}} / \beta_0}. \tag{26}$$

To further simplify the subsequent computational expressions, we can define the following two parameters:

$$a_m = e^{j\varphi_m^u} \sqrt{P_m^u \beta_m / \beta_0}, \tag{27}$$

$$b_m = e^{j\varphi_m^l} \sqrt{P_m^l \beta_m / \beta_0}. \tag{28}$$

Then, Eqs. (25) and (26) can be rewritten as

$$-\frac{\eta_0}{2\Lambda_y} [(1+R_m)(I_1^u e^{-j\xi_m d_1} + I_2^u + I_3^u e^{j\xi_m d_2}) + T_m (I_1^l e^{-j\xi_m d_3} + I_2^l e^{j\xi_m d_4})] + \delta_{m0} E_{\text{in}} R_0 = E_{\text{in}} a_m, \tag{29}$$

$$-\frac{\eta_0}{2\Lambda_y} [(1+R_m)(I_1^l e^{-j\xi_m d_3} + I_2^l e^{j\xi_m d_4}) + T_m (I_1^u e^{-j\xi_m d_1} + I_2^u + I_3^u e^{j\xi_m d_2})] + \delta_{m0} E_{\text{in}} T_0 = E_{\text{in}} b_m. \tag{30}$$

When $m = -1$, 0, and 1, the above Eqs. (29) and (30) can be expanded into six equations, which contain only five current parameters (I_1^u, I_2^u, I_3^u, I_1^l, and I_2^l). Therefore, when considering the power ratio of each propagating diffraction mode, i.e., when solving these equations, only five of them need to be arbitrarily chosen for the solution. The feasibility of this approach also implies the inherent property of metagratings, that is, controlling five diffraction modes is equivalent to controlling the whole six diffraction modes here.

Therefore, here we choose the −1st, 0th, and 1st reflection modes as well as the −1st and 0th transmission modes as our modes to be controlled, i.e., the five equations concluding Eq. (29) with $m=-1$, 0, 1 and Eq. (30) with $m=-1$, 0 are solved to get the five currents. For convenience in the subsequent derivation, here we define two radiative impedance density functions $Z^r(y,z)$ and $Z^t(y,z)$ as in Ref. [28] with respect to reflection and transmission, respectively, which are denoted as

$$Z^r(y,z)=j\frac{k_0\eta_0}{2\Lambda_y}\sum_{m=-\infty}^{+\infty}\frac{1+R_m}{\alpha_m}e^{-j\xi_m y}e^{-\alpha_m|z|}, \tag{31}$$

$$Z^t(y,z)=j\frac{k_0\eta_0}{2\Lambda_y}\sum_{m=-\infty}^{+\infty}\frac{T_m}{\alpha_m}e^{-j\xi_m y}e^{-\alpha_m|z|} \tag{32}$$

with $\alpha_m=j\beta_m=\sqrt{\xi_m^2-k_0^2}$. When $(y,z)=(0,0)$, Eq. (31) has a series divergence term and needs to be rewritten as [33]

$$Z^r(0,0)=\frac{\eta_0(1+R_0)}{2\Lambda_y\cos\theta_{\text{in}}}+j\frac{\eta_0}{\lambda_0}\left\{\ln\left(\frac{\Lambda_y}{2\pi r}\right)+\frac{1}{2}\sum_{\substack{m=-\infty\\ m\neq 0}}^{\infty}\left[\frac{2\pi(1+R_m)}{\Lambda_y\alpha_m}-\frac{1}{|m|}\right]\right\}, \tag{33}$$

where parameter r denotes the effective radius of the wires, as shown in Fig. 1(b).

Then combining Eqs. (19), (20), (31), (32), and Ohm's law $E_x^{\text{tot}}=ZI$, at the upper surface of the metagrating $(z=-h)$, we have

$$\begin{pmatrix}Z_1^uI_1^u\\ Z_2^uI_2^u\\ Z_3^uI_3^u\end{pmatrix}=\begin{bmatrix}E_{\text{in}}(1+R_0)\\ E_{\text{in}}(1+R_0)\\ E_{\text{in}}(1+R_0)\end{bmatrix}-Q_{3\times3}^{u(r)}\begin{pmatrix}I_1^u\\ I_2^u\\ I_3^u\end{pmatrix}-Q_{3\times2}^{l(t)}\begin{pmatrix}I_1^l\\ I_2^l\end{pmatrix} \tag{34}$$

with

$$Q_{3\times3}^{u(r)}=\begin{bmatrix}Z^r(0,0) & Z^r(d_1,0) & Z^r(d_1+d_2,0)\\ Z^r(d_1,0) & Z^r(0,0) & Z^r(d_2,0)\\ Z^r(d_1+d_2,0) & Z^r(d_2,0) & Z^r(0,0)\end{bmatrix}, \tag{35a}$$

$$Q_{3\times2}^{l(t)}=\begin{bmatrix}Z^t(d_1-d_3,0) & Z^t(d_1+d_4,0)\\ Z^t(d_3,0) & Z^t(d_4,0)\\ Z^t(d_2+d_3,0) & Z^t(d_2-d_4,0)\end{bmatrix}. \tag{35b}$$

Similarly, at the lower surface of the metagrating $(z=0)$, we have

$$\begin{pmatrix}Z_1^lI_1^l\\ Z_2^lI_2^l\end{pmatrix}=\begin{pmatrix}E_{\text{in}}T_0\\ E_{\text{in}}T_0\end{pmatrix}-Q_{2\times2}^{l(r)}\begin{pmatrix}I_1^l\\ I_2^l\end{pmatrix}-Q_{2\times3}^{u(t)}\begin{pmatrix}I_1^u\\ I_2^u\\ I_3^u\end{pmatrix} \tag{36}$$

with

$$Q_{2\times2}^{l(r)}=\begin{bmatrix}Z^r(0,0) & Z^r(d_3+d_4,0)\\ Z^r(d_3+d_4,0) & Z^r(0,0)\end{bmatrix}, \tag{37a}$$

$$Q_{2\times3}^{u(t)}=\begin{bmatrix}Z^t(d_1-d_3,0) & Z^t(d_3,0) & Z^t(d_2+d_3,0)\\ Z^t(d_1+d_4,0) & Z^t(d_4,0) & Z^t(d_2-d_4,0)\end{bmatrix}, \tag{37b}$$

where I_1^u, I_2^u, I_3^u, I_1^l, and I_2^l are the polarization currents and Z_1^u, Z_2^u, Z_3^u, Z_1^l, and Z_2^l are the load-impedance density of the five wires on the upper and lower surfaces of the metagrating.

Meanwhile, according to the system of Eqs. (29) and (30), the currents on the lower face of the metagrating can be derived as

$$I_s^l=\frac{\Lambda_y}{\eta_0}E_{\text{in}}p_s,\ (s=1,2) \tag{38}$$

with

$$p_1=\frac{2}{e^{j\xi_1d_3}-e^{-j\xi_1d_4}}\left[\frac{-(1+R_1)b_{-1}+T_1a_{-1}}{(1+R_1)^2-T_1^2}+\frac{(1+R_0)b_0-T_0(1+a_0)}{(1+R_0)^2-T_0^2}e^{-j\xi_1d_4}\right], \tag{39a}$$

$$p_2=\frac{2}{e^{j\xi_1d_3}-e^{-j\xi_1d_4}}\left[\frac{(1+R_1)b_{-1}-T_1a_{-1}}{(1+R_1)^2-T_1^2}-\frac{(1+R_0)b_0-T_0(1+a_0)}{(1+R_0)^2-T_0^2}e^{j\xi_1d_3}\right]. \tag{39b}$$

The currents on the upper face of the metagrating are derived as

$$I_s^u = \frac{\Lambda_y}{\eta_0} E_{\text{in}} q_s, \quad (s = 1, 2, 3) \tag{40}$$

with

$$q_1 = \frac{2}{(e^{j\xi_1 d_1} - 1)(e^{j\xi_1 d_2} - e^{-j\xi_1 d_1})} \times \left\{ \begin{array}{l} \dfrac{-(1+R_1)a_{-1} + T_1 b_{-1}}{(1+R_1)^2 - T_1^2} e^{j\xi_1 d_2} - \left[1 - \dfrac{(1+R_0)(a_0+1) - T_0 b_0}{(1+R_0)^2 - T_0^2}\right](1 + e^{j\xi_1 d_2}) - \dfrac{a_1}{1+R_1} \\ -\dfrac{T_1}{1+R_1}\left[\dfrac{(1+R_1)b_{-1} - T_1 a_{-1}}{(1+R_1)^2 - T_1^2} e^{j\xi_1(d_4-d_3)} - \dfrac{(1+R_0) - T_0 b_0(1+a_0)}{(1+R_0)^2 - T_0^2}(e^{-j\xi_1 d_3} + e^{j\xi_1 d_4})\right] \end{array} \right\}, \tag{41a}$$

$$q_2 = \frac{2}{(e^{j\xi_1 d_1} - 1)(e^{j\xi_1 d_2} - 1)} \times \left\{ \begin{array}{l} \dfrac{(1+R_1)a_{-1} - T_1 b_{-1}}{(1+R_1)^2 - T_1^2} e^{j\xi_1 d_2} + \left[1 - \dfrac{(1+R_0)(a_0+1) - T_0 b_0}{(1+R_0)^2 - T_0^2}\right](1 + e^{j\xi_1(d_1+d_2)}) + \dfrac{a_1 e^{j\xi_1 d_1}}{1+R_1} \\ +\dfrac{T_1 e^{j\xi_1 d_1}}{1+R_1}\left[\dfrac{(1+R_1)b_{-1} - T_1 a_{-1}}{(1+R_1)^2 - T_1^2} e^{j\xi_1(d_4-d_3)} - \dfrac{(1+R_0)b_0 - T_0(1+a_0)}{(1+R_0)^2 - T_0^2}(e^{-j\xi_1 d_3} + e^{j\xi_1 d_4})\right] \end{array} \right\}, \tag{41b}$$

$$q_3 = \frac{2}{(e^{j\xi_1 d_2} - 1)(e^{j\xi_1 d_1} - e^{-j\xi_1 d_2})} \times \left\{ \begin{array}{l} \dfrac{-(1+R_1)a_{-1} + T_1 b_{-1}}{(1+R_1)^2 - T_1^2} - \left[1 - \dfrac{(1+R_0)(a_0+1) - T_0 b_0}{(1+R_0)^2 - T_0^2}\right](1 + e^{j\xi_1 d_1}) - \dfrac{a_1 e^{j\xi_1 d_1}}{1+R_1} \\ -\dfrac{T_1 e^{j\xi_1 d_1}}{1+R_1}\left[\dfrac{(1+R_1)b_{-1} - T_1 a_{-1}}{(1+R_1)^2 - T_1^2} e^{j\xi_1(d_4-d_3)} - \dfrac{(1+R_0)b_0 - T_0(1+a_0)}{(1+R_0)^2 - T_0^2}(e^{-j\xi_1 d_3} + e^{j\xi_1 d_4})\right] \end{array} \right\}. \tag{41c}$$

After obtaining the analytical expression of the polarization currents, substituting them into Eqs. (34) and (36), respectively, we can obtain the closed form analytical solutions of wire load-impedance density as

$$Z_1^u = \frac{\eta_0}{\Lambda_y}\left(\frac{1+R_0}{q_1}\right) - Z^r(0,0) - j\frac{k_0\eta_0}{2\Lambda_y}\sum_{m=-\infty}^{+\infty}\left[\frac{1+R_m}{\alpha_m}\left(\frac{q_2}{q_1} + \frac{q_3}{q_1}e^{-j\xi_m d_2}\right) + \frac{T_m}{\alpha_m}\left(\frac{p_1}{q_1}e^{j\xi_m d_3} + \frac{p_2}{q_1}e^{-j\xi_m d_4}\right)\right]e^{-j\xi_m d_1}, \tag{42a}$$

$$Z_2^u = \frac{\eta_0}{\Lambda_y}\left(\frac{1+R_0}{q_2}\right) - Z^r(0,0) - j\frac{k_0\eta_0}{2\Lambda_y}\sum_{m=-\infty}^{+\infty}\left[\frac{1+R_m}{\alpha_m}\left(\frac{q_1}{q_2}e^{-j\xi_m d_1} + \frac{q_3}{q_2}e^{-j\xi_m d_2}\right) + \frac{T_m}{\alpha_m}\left(\frac{p_1}{q_2}e^{-j\xi_m d_3} + \frac{p_2}{q_2}e^{-j\xi_m d_4}\right)\right], \tag{42b}$$

$$Z_3^u = \frac{\eta_0}{\Lambda_y}\left(\frac{1+R_0}{q_3}\right) - Z^r(0,0) - j\frac{k_0\eta_0}{2\Lambda_y}\sum_{m=-\infty}^{+\infty}\left[\frac{1+R_m}{\alpha_m}\left(\frac{q_1}{q_3}e^{-j\xi_m d_1} + \frac{q_2}{q_3}\right) + \frac{T_m}{\alpha_m}\left(\frac{p_1}{q_3}e^{-j\xi_m d_3} + \frac{p_2}{q_3}e^{j\xi_m d_4}\right)\right]e^{-j\xi_m d_2}, \tag{42c}$$

$$Z_1^l = \frac{\eta_0}{\Lambda_y}\left(\frac{T_0}{p_1}\right) - Z^r(0,0) - j\frac{k_0\eta_0}{2\Lambda_y}\sum_{m=-\infty}^{+\infty}\left[\frac{1+R_m}{\alpha_m}\frac{p_2}{p_1}e^{-j\xi_m d_4} + \frac{T_m}{\alpha_m}\left(\frac{q_1}{p_1}e^{j\xi_m d_1} + \frac{q_2}{p_1} + \frac{q_3}{p_1}e^{-j\xi_m d_2}\right)\right]e^{-j\xi_m d_3}, \tag{42d}$$

$$Z_2^l = \frac{\eta_0}{\Lambda_y}\left(\frac{T_0}{p_2}\right) - Z^r(0,0) - j\frac{k_0\eta_0}{2\Lambda_y}\sum_{m=-\infty}^{+\infty}\left[\frac{1+R_m}{\alpha_m}\frac{p_1}{p_2}e^{-j\xi_m d_3} + \frac{T_m}{\alpha_m}\left(\frac{q_1}{p_2}e^{-j\xi_m d_1} + \frac{q_2}{p_2} + \frac{q_3}{p_2}e^{j\xi_m d_2}\right)\right]e^{-j\xi_m d_4}. \tag{42e}$$

To consider passive and lossless metagratings so as to ensure the maximum efficiency, we need an additional constraint on the load-impedance density, which is

$$\begin{aligned} &\mathrm{Re}[Z_1^u]=0, \quad \mathrm{Re}[Z_2^u]=0, \quad \mathrm{Re}[Z_3^u]=0, \\ &\mathrm{Re}[Z_1^l]=0, \quad \mathrm{Re}[Z_2^l]=0. \end{aligned} \tag{43}$$

Finally, the design of various types of beam manipulation can be completed by assigning values to parameters a_{-1}, a_0, a_1, b_{-1}, and b_0. From Eqs. (27) and (28), it can be seen that when the different a_m and b_m are determined, the corresponding different diffraction powers P_m^u and P_m^l are determined.

For the anomalous refraction, we let the +1st transmission diffraction mode as the radiated beam to realize anomalous refraction, meaning that we have

$$a_{-1}=a_0=a_1=b_{-1}=b_0=0. \tag{44}$$

Solving the system of Eqs. (43) and (44), the constellation parameters of the meta-atoms, i.e., d_1, d_2, d_3, d_4, and h, can be calculated. By substituting these parameters into the load-impedance density expressions (42a)–(42e), the required corresponding impedance density values of each meta-atom can be calculated.

For the anomalous reflection design, we consider the +1st reflection diffraction mode as the radiated beam. Thus, it can be obtained that

$$a_{-1}=a_0=b_{-1}=b_0=0, a_1=e^{j\varphi_1^u}\sqrt{\beta_1/\beta_0}. \tag{45}$$

Since an extra unknown φ_1^u is introduced in Eq. (45), we need to add an extra equation $|e^{j\varphi_1^u}|-1=0$ when solving the system of Eqs. (43) and (45) so that the number of unknowns d_1, d_2, d_3, d_4, h, and φ_1^u is the same as the number of equations, thus enabling the system of equations to be solved successfully. Similarly, the required impedance densities are calculated by substituting these solved parameters into the impedance density expressions.

In addition, it is worthwhile to note that when designing the metagratings, the Joule losses usually constitute an unavoidable factor affecting the efficiency. In particular, large amplitude polarization currents will cause significant losses, even though the real part of the load-impedance density of the meta-atom may be very small. By analyzing Eqs. (38) and (40), we can know that the amplitude of the currents is affected by the substrate thickness h. When the denominators in Eqs. (38) and (40) are zero, i.e., $\sin(\beta_s h)=0$, the current amplitudes will be infinite, and the corresponding thickness can be derived as

$$h=\frac{n}{2\sqrt{\varepsilon_r}}\lambda_0, (n=0,1,2\ldots). \tag{46}$$

It is worthwhile to note that we should not only avoid choosing the thickness of the substrate in Eq. (46), but also the values around it. Interestingly, this result is consistent with previous results when a supercell contains one meta-atom [16,17], as well as two meta-atoms [28]. So, we conclude that for a metagrating supercell containing arbitrary multiple meta-atoms, the nearby values of the substrate thickness in Eq. (46) need to be avoided.

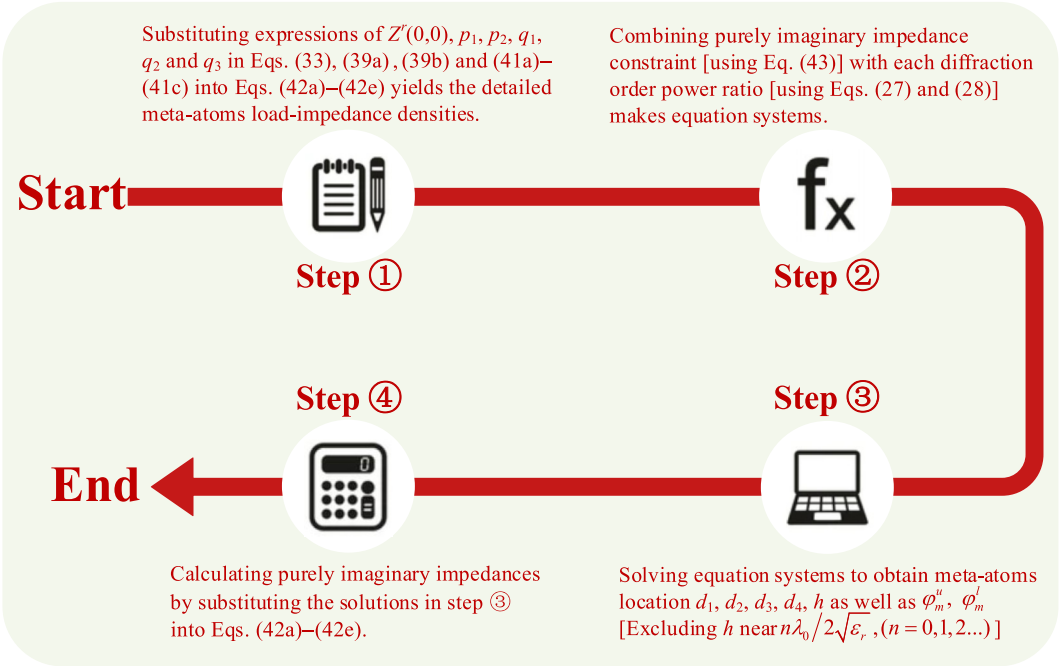

FIG. 2. Computational flowchart for fully analytical design of metagratings.

This corollary may be a convenient and direct reference in metagrating designs to avoid as much as possible losses caused by Joule heating. In order to have a more intuitive view of the analytical formulas proposed in this paper for the design of the metagratings, the calculation steps are summarized in the flowchart depicted in Fig. 2.

III. DESIGN, SIMULATIONS, AND EXPERIMENTS

To validate our proposed methodology, a proof-of-study study is numerically and experimentally reported for beam refraction and reflection schemes. The operating frequency of the metagrating is set to 10 GHz. Since the calculated reactance densities are all negative, and considering the practical feasibility of the model, the wires are replaced by meta-atoms with microstrip capacitor structures to achieve the required impedance density of the wires in the supercell, as shown in Fig. 3(a). The material of meta-atom is copper and the thickness and width or the microstrip wire are $t = 0.018$ mm and $w = 0.2$ mm, respectively. The capacitor's gap is $g = 0.2$ mm and width is L, which is obtained using an electromagnetic parameter retrieval procedure (see Appendix B for details). The dimensions of the metagrating supercell in the x direction and y direction are considered as $\Lambda_x = \lambda/10$ and $\Lambda_y = \lambda/\sin\theta_1$ (θ_1 is the angle of the +1st diffraction mode), respectively, as shown in Figs. 3(b) and 3(c). The dielectric substrate is selected as F4BM300 ($\varepsilon = 3\varepsilon_0$ and $\tan\delta = 0.0007$) with a thickness h.

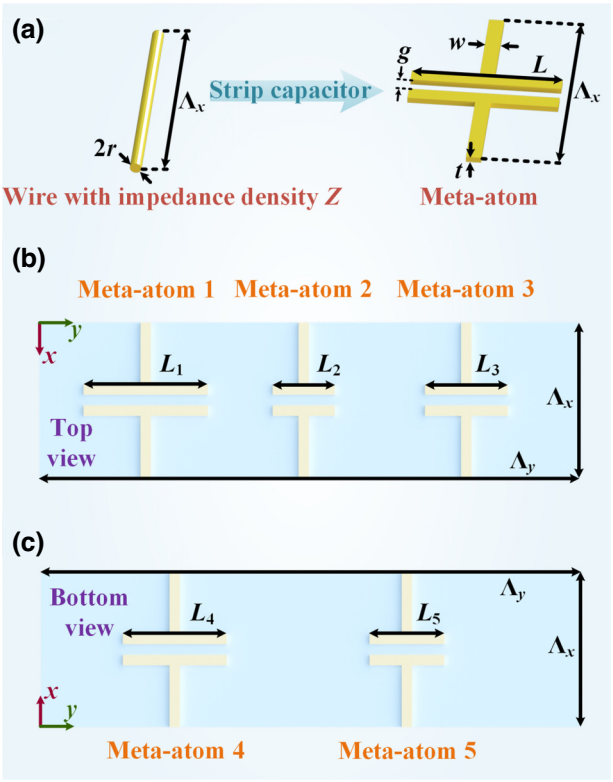

FIG. 3. (a) Realization of meta-atoms with reactive load-impedance density using microstrip line capacitor. (b) Top view of the metagrating supercell. (c) Bottom view of the metagrating supercell.

For the metagratings, we consider designs with 75° refraction and 70° reflection. Other angle designs of anomalous refraction and anomalous reflection are presented in Appendix C. Once the angle and power ratio of each diffraction order are determined, the constellation and the load-impedance density of each meta-atom in the supercell are calculated by Eqs. (43)–(45). The dimensions of the meta-atoms can then be determined and the final parameters of the metagrating supercells are given in Table I. The anomalous refraction and reflection diagrams of the metagratings are shown in Figs. 4(a) and 4(c), respectively, and the simulated performances of the corresponding supercells are depicted in Figs. 4(b) and 4(d). From the results, it can be observed that for both designs the energy is almost completely transformed from the incident wave to the desired outgoing wave at 10 GHz, with less than 0.4% of the power radiated in the direction of parasitic scattering. The inevitable Joule losses are of the order of 6.24% for the anomalous refraction and 10.95% for the anomalous reflection. The reason for more power absorption in the anomalous reflection design is that the thickness of its substrate is closer to the value of h in Eq. (46), and thus the larger amplitude of the polarization current leads to more Joule heat losses. It is worthwhile to note that some multispace harmonic metasurface designs using the "phase-shift" approach have also been proposed to achieve efficient wavefront manipulation [34–36]. However, most of them rely on densely arranged meta-atoms and on full-wave optimizations, therefore lacking intuitive design

TABLE I. Parameters of the metagratings with 75° anomalous refraction and 70° anomalous reflection.

Parameters \ Supercell type	Anomalous refraction	Anomalous reflection
Λ_x (mm)	3	3
Λ_y (mm)	31.06	31.93
h (mm)	2.37	7.42
d_1 (mm)	10.90	11.30
d_2 (mm)	13.14	10.94
d_3 (mm)	11.19	9.74
d_4 (mm)	12.33	10.48
$Z_1^u(\eta/\lambda)$	$-j\,3.7060$	$-j\,2.2093$
$Z_2^u(\eta/\lambda)$	$-j\,1.5637$	$-j\,4.1663$
$Z_3^u(\eta/\lambda)$	$-j\,4.0354$	$-j\,2.7461$
$Z_1^l(\eta/\lambda)$	$-j\,4.4263$	$-j\,4.1104$
$Z_2^l(\eta/\lambda)$	$-j\,4.3434$	$-j\,4.1231$
L_1 (mm)	4.22	5.89
L_2 (mm)	6.92	3.85
L_3 (mm)	3.96	5.19
L_4 (mm)	3.67	3.89
L_5 (mm)	3.72	3.88

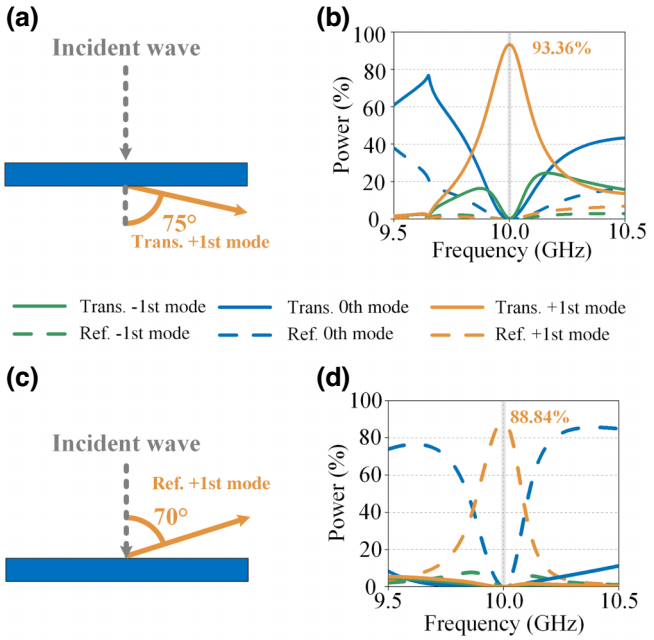

FIG. 4. Different beam-manipulation diagram: (a) anomalous refraction, (c) anomalous reflection. Simulation results of the supercells: (b) anomalous refraction, (d) anomalous reflection.

guidance. Hence, metagratings with sparsely arranged meta-atoms designed by explicit analytical design guidance constitute an excellent alternative for efficient wavefront manipulation.

To further verify the validity of the proposed design methodology through experiments, the parameters listed in Table I are used to fabricate the two metagratings using classical PCB technology, as shown by the photographs in Figs. 5(a) and 5(b). The two proof-of-concept prototypes, both consisting of 100×18 supercells in x and y direction, respectively, i.e., 300 mm $\times$ 574.74 and 300 mm $\times$ 559.08 mm, are measured using the experimental setup shown in Fig. 5(c). The metagrating under test is mounted on a low-index foam support surrounded by microwave absorbing materials, and three standard horn antennas are utilized for the measurements. The transmitter antenna is placed away from the prototype at a distance of 2.5 m to launch a quasiplanar wave-front illumination. The receiving antenna 1 and the receiving antenna 2 are mounted on two rotatable mechanical arms to record the scattered waves from the metagrating plate at a distance of 2.5 m as well as 2 m away from the plate, respectively. Finally, the measurement is accomplished by keeping the transmitter and the metagrating fixed and rotating the mechanical arms with 1° step.

Figure 6(a) compares the simulated and measured normalized far-field scattered power of the metagratings at 10 GHz. In addition to very small angular errors, the metagratings are able to redirect the incident wave toward the predicted angles well. For the 75° anomalous refraction design, the simulation shows a main beam pointing at 73°, while the measurement shows a refraction to 74°. For the 70° anomalous reflection design, both simulation and measurement show a main beam pointing at 69°. The observed angular deviations are due to the finite size of the metagrating samples. In order to minimize the deviation with respect to the theoretically expected value, the size of the samples need to be increased as much as possible. The diffraction efficiency η_{sca}, which is the ratio of the power in the direction of the outgoing beam to the total diffracted power of the metagrating, is given as [20]

$$\eta_{\text{sca}} = \frac{\int_{\theta_m^1}^{\theta_m^2} P(\theta)d\theta}{\sum_m \int_{\theta_m^1}^{\theta_m^2} P(\theta)d\theta}, \tag{47}$$

where $P(\theta)$ is the power scattered at angle θ, and θ_m^1 and θ_m^2 are the angles where the scattered power is 3 dB less than

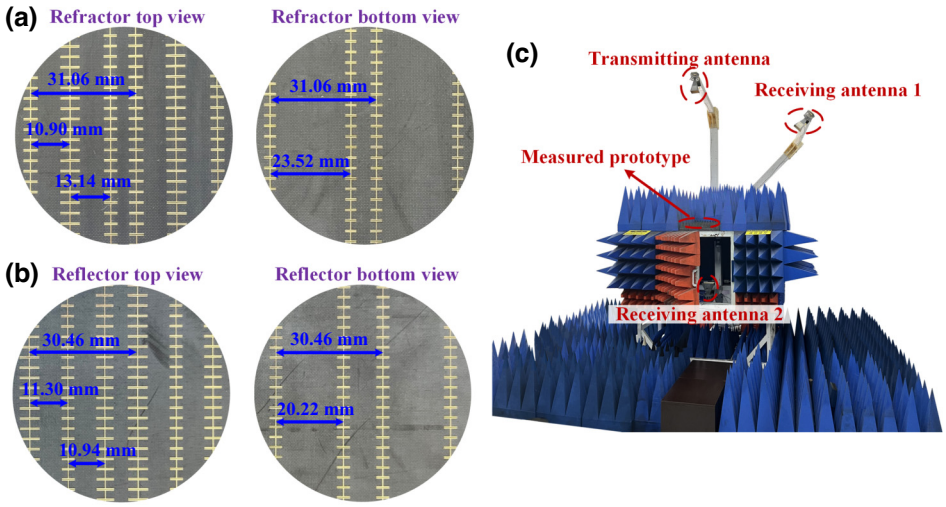

FIG. 5. Enlarged view on two lateral and multiple longitudinal periods of the fabricated metagrating plates, the sizes as well as spacing of the meta-atoms are labeled in blue: (a) anomalous refractor, (b) anomalous reflector. (c) Experimental setup, consists of one transmitter and two receiver standard horn antennas, and rotatable arms.

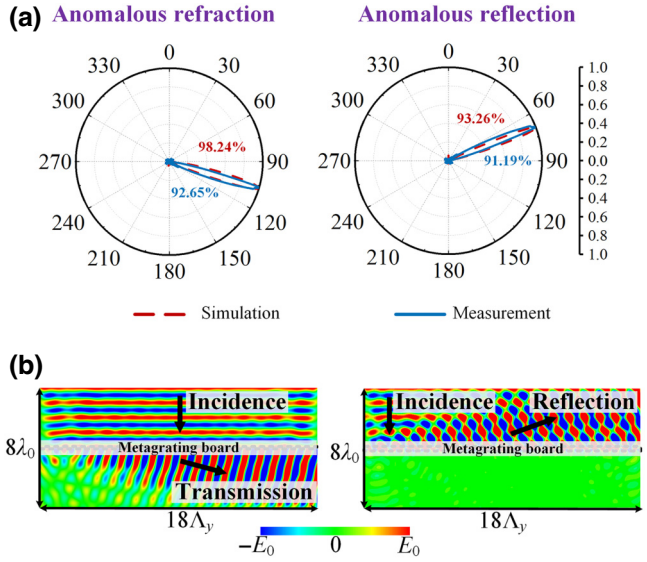

FIG. 6. Far-field simulation and measurement results of the fabricated metagrating anomalous refractor and anomalous reflector. Near-field simulation result of the fabricated metagrating anomalous refractor and anomalous reflector.

the peak value in the direction of the mth diffraction order. The simulated and measured diffraction efficiency for the 75° anomalous refraction metagrating is then found to be 98.24% and 92.65%, respectively. For the 70° anomalous reflection, the diffraction efficiency is 93.26% and 91.19%, in simulation and experiment, respectively. It should be noted that for the total efficiency, Joule losses as well as the edge effects of the board contribute to the power loss [17]. Finally, the near-field distribution extracted from full-wave simulations, displayed in Fig. 6(b), show that when the incident waves pass through the metagrating board, they both point to the expected angle. Particularly, for the anomalous reflection, it is interesting to observe that no energy is transmitted on the bottom side of the metagrating, even if there is no ground plane.

IV. CONCLUSION

In summary, we have proposed a fully analytical methodology to design groundless transmissive electromagnetic metagratings for highly efficient extreme-angle beam manipulation. Unlike the designs achieved with the help of optimization algorithms, here we derive closed-form formulas to obtain the required impedance density of the meta-atoms. The proposed methodology constitutes a convenient and straightforward design tool for a future extreme-angle beam-manipulation scheme based on metagratings. The validity of the proposed methodology is numerically and experimentally validated for large-angle anomalous reflection and refraction configurations. Moreover, it is particularly noted that high-efficiency reflection can be obtained from a metagrating topology without ground plane, suggesting that it can be further exploited for out-of-band transmission features. The proposed metagratings can be good alternatives for future applications in base stations, satellite terminals, and lens antennas for edge coverage enhancement.

ACKNOWLEDGMENTS

This work is supported by the China Scholarship Council under Grant No. 202206280099.

APPENDIX A: DISCUSSION ABOUT THE PERIOD LENGTH SELECTION FOR THE METAGRATINGS

Here, we mainly consider beam manipulation of transmissive metagratings under a normal incidence, i.e., $\theta_{\text{in}}=0°$. First, we discuss the effect of the metagratings period length Λ_y on the angular range of the beam manipulation. Since the incidence is normal, the number of transmission or reflection diffraction modes will be odd, i.e., $2|m|+1=3, 5, 7\ldots$ (m denotes the mth transmission and reflection diffraction order). For the sake of simplicity, let us use the transmission diffraction modes as an example (the reflection diffraction modes are symmetrical to the transmission ones, and they have the same angular range), as shown in Fig. 7. If $\lambda_0 < \Lambda_y < 2\lambda_0$, there are only three transmission diffraction modes, i.e., $m=1$, and the diffraction angle of the $+1$st order is $\theta_1 = \arcsin(\xi_{+1}/k_0)$, as shown in Fig. 7(a). Thus, if we select the $+1$st order as the anomalous refraction beam, the beam-manipulation range is equal to the range of θ_1, which is

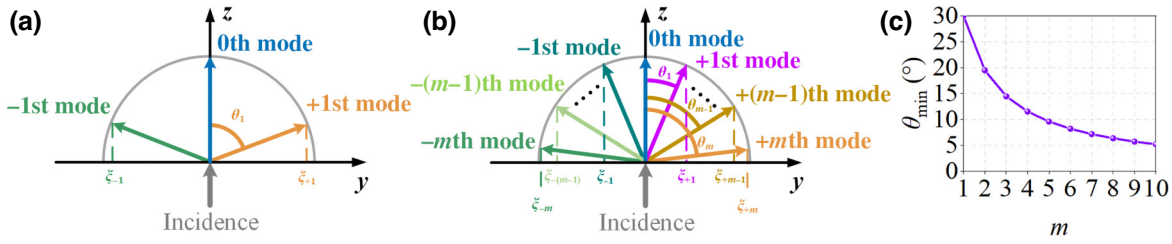

FIG. 7. Wave-vector diagram of different transmission Floquet modes of the transmissive metagratings: (a) three modes, (b) $2|m|+1$ modes, (c) $\theta_{\min}$ under different maximum diffraction order m.

$30° < \theta_1 < 90°$. As shown in Fig. 7(b), when the range of the period Λ_y becomes $m\lambda_0 < \Lambda_y < (m+1)\lambda_0$, the metagrating has more transmission diffraction modes, i.e., $2m+1$ diffraction modes. Then, the range of anomalous refraction on the right side will include all the ranges from θ_1 to θ_m, where θ_m is the diffraction angle of $+m$th order. The maximum angle of anomalous refraction is $\theta_{\max} = 90°$, and the minimum angle of anomalous refraction is $\theta_{\min} = \arcsin[1/(m+1)]$, and the relationship of $\theta_{\min}$ with m is shown in Fig. 7(c). From the above analysis, we can know that as the number of diffraction modes increases, the maximum angle of anomalous refraction is always kept at 90°, while the mnimum angle changes from 30° toward to 5° and the change trend gradually becomes slower, which can be seen in Fig. 7(c). Thus, here for metagratings focusing on the large-angle beam manipulation, choosing $\lambda_0 < \Lambda_y < 2\lambda_0$ is sufficient to meet the requirement for the extreme-angle beam manipulation.

APPENDIX B: OBTAINING META-ATOMS' SIZE CORRESPONDING TO THE REQUIRED LOAD-IMPEDANCE DENSITY USING *S*-PARAMETER RETRIEVAL

For the meta-atom load-impedance density at a certain frequency, it can be obtained either by the analytical formulas given in Ref. [28] or by the local periodic approximation method poposed by Popov *et al.* [21]. In this paper, since the supercell contains more than one meta-atom, we choose the more accurate parameter extraction method [21]. Considering the completeness, here we briefly describe the derivation of the *S*-parameter retrieval procedure.

As shown in Fig. 8, we build the desired meta-atom structure in HFSS simulation software. In this model, the height of the air box with periodic boundary condition is λ_0, and Floquet port 1 is used as an excitation port on the top face of the air box. The permittivity of the dielectric substrate is the same as in Sec. II ($\varepsilon = 3\varepsilon_0$ and tan $\delta = 0.0007$). The width of the unit cell is $L_x = \lambda_0/10$. The length L_y of the unit cell can be taken arbitrarily, and to ensure that only 0th diffraction mode exists, here we consider $L_y = \lambda_0/2$. The thickness of the substrate h can also be taken arbitrarily, just to ensure that it is away from h given in formula (62), here we consider $h = \lambda_0/10$. The width of the microstrip capacitor trace is considered to be $w = 0.2$ mm as in Sec. II. Considering the same illumination as in Sec. II, the electric field amplitude of the reflection 0th mode E_0 in Fig. 8 is [37]

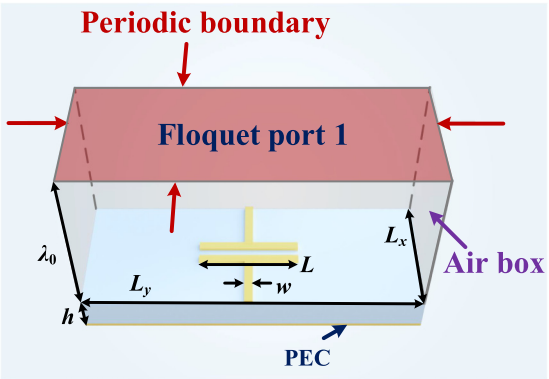

FIG. 8. Model built for HFSS simulation to extract the load-impedance density of meta-atoms.

$$E_0 = -\frac{k_0\eta_0}{2L_y}\left(\frac{1+R'_0}{\beta_0}\right)I_0 + E_{\text{in}}R'_0, \tag{B1}$$

where $R'_0 = \left[\tan(k_s h) + j\sqrt{\varepsilon_r}\right]/\left[\tan(k_s h) - j\sqrt{\varepsilon_r}\right]$ is the Fresnel reflection coefficient of the incident wave. Then the load-impedance density of the meta-atom can be expressed as [37]

$$Z = \frac{\eta_0}{2L_y}\left[\frac{(1+R'_0)^2}{R'_0 E_{\text{in}} - E_0}\right] - Z(0,0) \tag{B2}$$

with

$$Z(0,0) = \frac{\eta_0}{2L_y}T'_0 + j\frac{\eta_0}{\lambda_0}\left[\ln\left(\frac{2L_y}{\pi w}\right) + \sum_{m=1}^{\infty}\left(\frac{2\pi T'_m}{L_y\alpha_m} - \frac{1}{m}\right)\right], \tag{B3}$$

where $T'_m = 2\tanh(\alpha'_m h)/[\tanh(\alpha'_m h) + \alpha'_m/\alpha_m]$, $\alpha_m = k_0\sqrt{(m\lambda_0/L_y)^2 - 1}$, and $\alpha'_m = k_0\sqrt{(m\lambda_0/L_y)^2 - \varepsilon_r}$.

In Fig. 8, when $E_{\text{in}} = 1$ V/m, then the E_0 can be written as $E_0 = E_{\text{in}}S_{11}e^{j\beta_0\lambda_0} = S_{11}e^{jk_0\lambda_0} = S_{11}$, where S_{11} is the scattering parameter of the Floquet port 1. Thus, we can obtain E_0 by extracting S_{11}. By scanning parameter L, the real and imaginary parts of different E_0 are obtained shown in Fig. 9(a). Then, the corresponding load-impedance density Z can be obtained according to Eq. (B2), as shown in

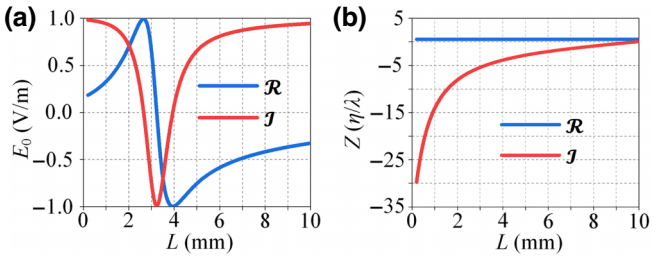

FIG. 9. Extracted real and imaginary parts of E_0 with different capacitor width L when $E_{\text{in}} = 1$ V/m, (b) calculated impedance density Z of the meta-atom with different capacitor width L according to extracted E_0.

TABLE II. Parameters of the metagratings with four types of beam manipulation.

Parameters \ Supercell type	Type A	Type B	Type C	Type D
Λ_x (mm)	3	3	3	3
Λ_y (mm)	46.67	36.62	52.30	39.16
h (mm)	5.38	4.92	5.91	6.73
d_1 (mm)	19.49	15.62	29.99	17.69
d_2 (mm)	14.09	6.85	5.43	10.10
d_3 (mm)	10.98	15.78	21.50	15.94
d_4 (mm)	16.33	5.04	13.12	9.36
$Z_1^u(\eta/\lambda)$	$-j$ 3.3.2735	$-j$ 4.1722	$-j$ 3.3967	$-j$ 2.7271
$Z_2^u(\eta/\lambda)$	$-j$ 1.9174	$-j$ 5.7574	$-j$ 4.2235	$-j$ 2.2666
$Z_3^u(\eta/\lambda)$	$-j$ 4.8696	$-j$ 5.0165	$-j$ 1.7130	$-j$ 2.9990
$Z_1^l(\eta/\lambda)$	$-j$ 4.4599	$-j$ 4.1319	$-j$ 3.7493	$-j$ 5.1017
$Z_2^l(\eta/\lambda)$	$-j$ 5.2848	$-j$ 6.2141	$-j$ 4.4473	$-j$ 4.8624
L_1 (mm)	4.61	3.82	4.51	5.21
L_2 (mm)	6.32	2.88	3.80	5.80
L_3 (mm)	3.37	3.27	6.65	4.91
L_4 (mm)	3.64	3.85	4.18	3.23
L_5 (mm)	3.13	2.67	3.64	3.38

[a]Type A: anomalous refraction at 40°.
[b]Type B: anomalous refraction at 55°.
[c]Type C: anomalous reflection at 35°.
[d]Type D: anomalous reflection at 50°.

Fig. 9(b), and the extracted real part of the impedance density is Re $[Z_q] = 0.5\eta/\lambda$, which is not considered here. For the imaginary impedance density required for each meta-atom in the metagrating, we can retrieve the corresponding capacitor width L. It should be noted that since the strategy used here to extract the meta-atom impedance density is based on the assumption that the entire metagrating periodic array is uniform (each reflective supercell contains one meta-atom), but the metagrating array designed in Sec. II is not uniform (each transmissive supercell contains five nonuniformly arranged meta-atoms). Owing to different interaction between adjacent meta-atom, it is also necessary to multiply the capacitor width by a correction factor K, which can be obtained by parameter sweeping in simulation. For the anomalous refraction and anomalous reflection metagratings in Sec. II, their correction factors are $K_{\text{refraction}} = 1.02$ and $K_{\text{reflection}} = 1.019$, respectively. Finally, the capacitor length L of the meta-atoms to realize different required load-impedance densities can be obtained and tabulated in Table I.

APPENDIX C: OTHER ANGLE DESIGNS OF ANOMALOUS REFRACTION AND REFLECTION

In Sec. III, we design an anomalous refraction with 75° and an anomalous reflection with 70°. Here, we will perform some other angle designs of anomalous refraction and reflection. The designs also follow Eqs. (44) and (45). Then, the parameters of these metagrating supercells are calculated and presented in Table II.

The anomalous refraction diagram for each type of metagrating is shown in Figs. 10(a) and 10(c) and the

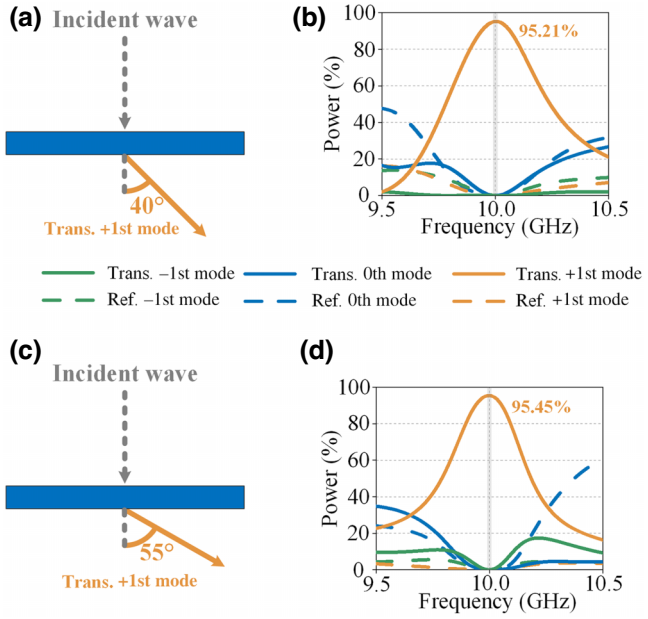

FIG. 10. Different anomalous refraction diagram: (a) type A, (c) type B; simulation results of the supercells: (b) type A, (d) type B.

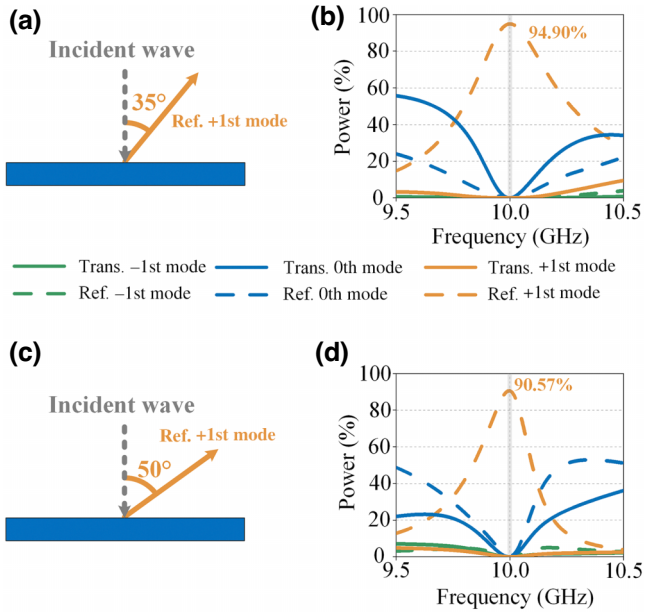

FIG. 11. Different anomalous reflection diagram: (a) type C, (c) type D; simulation results of the supercells: (b) type C, (d) type D.

simulated performances of the corresponding supercells are depicted in Figs. 10(b) and 10(d). It can be observed that for different anomalous refraction, the efficiency is higher than 95% (type A, 95.21%; type B, 95.45%), with less than 0.3% of the power radiated in the direction of parasitic scattering (type A, 0.25%; type B, 0.10%), and the remaining power is absorbed due to the inevitable Joule losses (type A, 4.54%; type B, 4.45%).

The anomalous reflection diagram for each type of metagratings are shown in Figs. 11(a) and 11(c), and the simulated performances of the corresponding supercells are depicted in Figs. 11(b) and 11(d). From the simulation results, the efficiency of each anomalous reflection reaches over 90% (type C, 94.90%; type D, 90.57%), with less than 0.5% of the power coupled to the parasitic scattering (type C, 0.17%; type D, 0.42%), and the remaining power is absorbed (type C, 4.93%; type D, 9.01%).

[1] Z. Cao, Q. Ma, A. B. Smolders, Y. Jiao, M. J. Wale, C. W. Oh, H. Wu, and A. M. J. Koonen, Advanced integration techniques on broadband millimeter-wave beam steering for 5G wireless networks and beyond, IEEE J. Quantum Electron. **52**, 1 (2016).

[2] R. Yonezawa, Y. Konishi, I. Chiba, and T. Katagi, Beam-shape correction in deployable phased arrays, IEEE Trans. Antennas Propag. **47**, 482 (1999).

[3] D. R. Smith, J. B. Pendry, and M. C. K. Wiltshire, Metamaterials and negative refractive index, Science **305**, 788 (2004).

[4] C. L. Holloway, E. F. Kuester, J. A. Gordon, J. O'Hara, J. Booth, and D. R. Smith, An overview of the theory and applications of metasurfaces: The two-dimensional equivalents of metamaterials, IEEE Antennas Propag. Mag. **54**, 10 (2012).

[5] N. Yu, P. Genevet, M. A. Kats, F. Aieta, J.-P. Tetienne, F. Capasso, and Z. Gaburro, Light propagation with phase discontinuities: generalized laws of reflection and refraction, Science **334**, 333 (2011).

[6] N. Mohammadi Estakhri and A. Alù, Wave-front transformation with gradient metasurfaces, Phys. Rev. X **6**, 041008 (2016).

[7] C. Pfeiffer and A. Grbic, Metamaterial Huygens' surfaces: Tailoring wave fronts with reflectionless sheets, Phys. Rev. Lett. **110**, 197401 (2013).

[8] A. Epstein and G. V. Eleftheriades, Huygens' metasurfaces via the equivalence principle: Design and applications, J. Opt. Soc. Am. B **33**, A31 (2016).

[9] A. Epstein and G. V. Eleftheriades, Floquet-Bloch analysis of refracting Huygens metasurfaces, Phys. Rev. B **90**, 235127 (2014).

[10] A. Epstein and G. V. Eleftheriades, Passive lossless huygens metasurfaces for conversion of arbitrary source field to directive radiation, IEEE Trans. Antennas Propag. **62**, 5680 (2014).

[11] C. Qi and A. M. H. Wong, Discrete Huygens' metasurface: Realizing anomalous refraction and diffraction mode circulation with a robust, broadband and simple design, IEEE Trans. Antennas Propag. **70**, 7300 (2022).

[12] A. Epstein and G. V. Eleftheriades, Synthesis of passive lossless metasurfaces using auxiliary fields for reflectionless beam splitting and perfect reflection, Phys. Rev. Lett. **117**, 256103 (2016).

[13] Y. Ra'di, D. L. Sounas, and A. Alù, Metagratings: Beyond the limits of graded metasurfaces for wave front control, Phys. Rev. Lett. **119**, 067404 (2017).

[14] Y. Raadi and A. Alu, Metagratings for efficient wavefront manipulation, IEEE Photonics J. **14**, 1 (2022).

[15] A. Epstein and O. Rabinovich, Unveiling the properties of metagratings via a detailed analytical model for synthesis and analysis, Phys. Rev. Appl. **8**, 054037 (2017).

[16] O. Rabinovich and A. Epstein, Analytical design of printed circuit board (PCB) metagratings for perfect anomalous reflection, IEEE Trans. Antennas Propag. **66**, 4086 (2018).

[17] O. Rabinovich, I. Kaplon, J. Reis, and A. Epstein, Experimental demonstration and in-depth investigation of analytically designed anomalous reflection metagratings, Phys. Rev. B **99**, 125101 (2019).

[18] G. Xu, S. V. Hum, and G. V. Eleftheriades, Dual-band reflective metagratings with interleaved meta-wires, IEEE Trans. Antennas Propag. **69**, 2181 (2021).

[19] V. Popov, F. Boust, and S. N. Burokur, Controlling diffraction patterns with metagratings, Phys. Rev. Appl. **10**, 011002 (2018).

[20] V. Popov, F. Boust, and S. N. Burokur, Constructing the near field and far field with reactive metagratings: Study on the degrees of freedom, Phys. Rev. Appl. **11**, 024074 (2019).

[21] V. Popov, M. Yakovleva, F. Boust, J.-L. Pelouard, F. Pardo, and S. N. Burokur, Designing metagratings via local

periodic approximation: From microwaves to infrared, Phys. Rev. Appl. **11**, 044054 (2019).
[22] V. Popov, F. Boust, and S. N. Burokur, Beamforming with metagratings at microwave frequencies: Design procedure and experimental demonstration, IEEE Trans. Antennas Propag. **68**, 1533 (2020).
[23] O. Rabinovich and A. Epstein, Nonradiative subdiffraction near-field patterns using metagratings, Appl. Phys. Lett. **118**, 131105 (2021).
[24] Y. Yashno and A. Epstein, Broad-angle multichannel metagrating diffusers, IEEE Trans. Antennas Propag. **71**, 2409 (2023).
[25] O. Rabinovich and A. Epstein, Arbitrary diffraction engineering with multilayered multielement metagratings, IEEE Trans. Antennas Propag. **68**, 1553 (2020).
[26] G. Xu, G. V. Eleftheriades, and S. V. Hum, Analysis and design of general printed circuit board metagratings with an equivalent circuit model approach, IEEE Trans. Antennas Propag. **69**, 4657 (2021).
[27] Z. Tan, J. Yi, S. Wang, X. Chen, and S. N. Burokur, Closed-form analytical design of a beamforming reflective metagrating with a relatively low number of meta-atoms, Opt. Mater. Express **13**, 624 (2023).
[28] Z. Tan, J. Yi, X. Chen, M. Lin, Z. H. Jiang, D. H. Werner, and S. N. Burokur, Fully analytical design of dual-wire PCB metagratings for beam steering and splitting, IEEE Trans. Antennas Propag. **71**, 5452 (2023).
[29] Z. Tan, J. Yi, V. Popov, and S. N. Burokur, Efficient beam splitting using zero-load-impedance metagratings, Opt. Lett. **48**, 3275 (2023).
[30] A. Casolaro, A. Toscano, A. Alu, and F. Bilotti, Dynamic beam steering with reconfigurable metagratings, IEEE Trans. Antennas Propag. **68**, 1542 (2020).
[31] Y. Kerzhner and A. Epstein, Metagrating-assisted high-directivity sparse regular antenna arrays for scanning applications, IEEE Trans. Antennas Propag. **71**, 650 (2023).
[32] J. Lin, G. Wang, S. Atapattu, R. He, G. Yang, and C. Tellambura, Transmissive metasurfaces assisted wireless communications on railways: Channel strength evaluation and performance analysis, IEEE Trans. Commun. **71**, 1827 (2023).
[33] S. Tretyakov, *Analytical Modeling in Applied Electromagnetics* (Artech House, Norwood, MA, USA, 2003).
[34] A. Díaz-Rubio, V. S. Asadchy, A. Elsakka, and S. A. Tretyakov, From the generalized reflection law to the realization of perfect anomalous reflectors, Sci. Adv. **3**, e1602714 (2017).
[35] H. W. Tian, X. G. Zhang, W. X. Jiang, X. Li, Y. K. Liu, C. Qiu, and T. J. Cui, Programmable controlling of multiple spatial harmonics via a nonlinearly phased grating metasurface, Adv. Funct. Mater. **32**, 2203120 (2022).
[36] Y. Wang, Y. Yuan, Y. Liu, X. Ding, B. Ratni, Q. Wu, S. N. Burokur, G. Hu, and K. Zhang, Extreme diffraction management in phase-corrected gradient metasurface by Fourier harmonic component engineering, Laser Photonics Rev. **17**, 2300152 (2023).
[37] Z. Tan, J. Yi, Q. Cheng, and S. N. Burokur, Design of perfect absorber based on metagratings: Theory and experiment, IEEE Trans. Antennas Propag. **71**, 1832 (2023).